Paleosol marked by contrasting formation processes: A pilot study using digital morphometrics in Southeastern Brazil

Fernanda Almeida Bócoli [a], Sérgio Henrique Godinho Silva [a], Junior Cesar Avanzi [a], Bruno Montoani Silva [a], Vanêssa Lopes de Faria [a], Maria Cecília Vieira Totti [a], Alberto Vasconcellos Inda [b], Gustavo Frosi [b], Suane de Souza Franco Lima [b], Alexandre Uezu [c], Marco Aurélio Carbone Carneiro [a], Marta Vasconcelos Ottoni [d], Nilton Curi [a,*]

[a] Department of Soil Science, Federal University of Lavras, Lavras, Minas Gerais 37.200-900, Brazil
[b] Department of Soils, Agronomy Faculty, Federal University of Rio Grande do Sul, Porto Alegre, Rio Grande do Sul 90.001-970, Brazil
[c] Faculty for Environmental Conservation and Sustainability (ESCAS), IPÊ—Institute for Ecological Research, 47 km of Dom Pedro I highway, Nazaré Paulista, São Paulo 12960-000, Brazil
[d] Department of Hydrology, Geological Survey of Brazil (SGB), Rio de Janeiro, RJ, Brazil

A B S T R A C T

Although soil formation results from the interactions of five classical factors and various pedogenic processes, such interactions can drastically change over time, which may be recorded in the so-called Paleosols. These soils may be formed under contrasting environmental conditions. Given such soils are rare in Brazil, this pilot study aimed to detail the morphological, physical, chemical (including elemental content and magnetic susceptibility (MS)), and mineralogical properties of a Paleosol with contrasting paleo- and current-drainage conditions, derived from sandstone having pellitic (fine) sediments intermixed, with support via digital morphometrics. Samples were collected in a regular grid of 15x15 cm along the soil profile down to 1.8 m depth. The soil samples were analyzed via portable X-ray fluorescence (pXRF) spectrometry and for assessment of magnetic susceptibility (MS), texture, fertility, and organic matter content. The mineralogy of the clay, silt, and sand fractions were determined via X-ray diffraction analyses. The pXRF and MS results were spatialized to the Paleosol profile. The first 108 cm of the soil profile are well-drained having reddish colors, contrasting with the underlying poorly-drained unity having greyish colors. The MS values were higher in the first 108 cm of the soil profile, reaching the lowest values in the 2Cg horizon at 142–180 cm depth. Quartz was the main mineral in sand and silt fractions, while kaolinite largely dominates the clay fraction in association with hematite. In the 2Cg horizon, the absence of hematite is related with the paleoredoximorphic conditions there. The Ti/Zr ratio indicated differences in parent materials of the reddish and greyish units of the Paleosol. The midslope position of the Paleosol makes colluvial deposition unlikely. The combined use of pXRF, MS, morphological, physical, chemical, and mineralogical analyses provided valuable details on the variation of the contrasting formation processes of the Paleosol studied.

1. Introduction

Soil systems are complex, resulting from the interactions among the soil forming factors (Jenny, 1941) coupled with specific pedogenic processes (Phillips, 2016; Schaetzl and Anderson, 2005). Although changes caused by these interactions occur continually in time, some soils have conserved features anciently developed during their formation; they are the so-called Paleosols. The concept adopted in this paper considers a Paleosol as a soil that formed on a landscape in the past, with distinctive morphological properties resulting from a soil-forming environment that no longer exists at the site (Soil Science Society of America, 2008). Paleosols can help in describing paleoenvironments, paleoclimates, evidences of old geomorphological surfaces, paleopedogenic processes, and inferences about the paleoarchaeology (Ladeira, 2010).

In Brazil, the records of Paleosols are rare (Stevanato et al., 2021).

Previous studies have been conducted in south and southeastern regions (Nascimento et al., 2017; Silva et al., 2017). Such soils are more commonly found in places that have undergone more recent glaciation, active volcanism or tectonism, climate change, high fluctuations of the sea level, and ancient alluvial or lacustrine deposition (Ladeira, 2010; Wright, 1992), among others.

Given the increasing variety of new tools to characterize soils, new approaches have emerged to investigate a soil profile in more detail, such as the digital soil morphometrics. This approach has provided different perspectives on the detailed study of soil profiles (Hartemink and Minasny, 2014). Thus, proximal sensors have allowed additional insights on soil genesis besides the spatial variation of soil properties within a soil profile (Grauer-Gray and Hartemink, 2018; Mancini et al., 2021; Silva et al., 2018; Sun et al., 2020).

Among the proximal sensors, portable X-ray fluorescence (pXRF) spectrometry and magnetic susceptibility (MS) measurements have been capable of refining the variability of morphological properties within and in between soil horizons (Bócoli et al., 2023; Grauer-Gray and Hartemink, 2018; Mancini et al., 2021; Silva et al., 2018; Sun et al., 2020). While the former delivers elemental contents present in the samples, the latter measures the magnetic susceptibility, which is related to soil mineralogy, especially ferrimagnetic minerals, such as magnetite and maghemite (Curi et al., 1984). These properties may be related to several other features of soils besides factors and processes of formation (Mello et al., 2020).

Due to intense erosion, mainly associated to humid conditions, the Brazilian landscape has substantially changed over time, including interruptions in the geological column in some states (Resende et al., 2019). So, some soils are located on current landscapes, which are in disagreement with their morphology. In this study, the redoximorphic features below the reddish A and B horizons (0–108 cm) are anomalous with the midslope position of the soil studied, raising the possibility of this unity (portion of the soil profile) may be formed under a more gentle paleorelief, in which the water table was high in the soil profile. Subsequent landscape dissection and drainage improvement may explain the current overlying reddish unity. The ancient redoximorphic processes in the soil profile supports the interpretation of a Paleosol (Soil Science Society of America, 2008).

This pilot study aims to detail the characterization of properties related to the contrasting pedogenesis processes of a Paleosol profile, containing hydromorphic features at the lower part of the profile, contrasting with overlying well-drained soil horizons, derived from sandstone with pellitic sediments intermixed, in Southeastern Brazil, through a combination of morphological, physical, chemical, mineralogical, and proximal sensors (pXRF and MS) analyses. The main hypothesis is that the combination of such techniques, via digital soil morphometrics, may provide additional details to field morphology, highlighting the understanding of the paleo- and current-soil forming processes involved. The novelty of this study encompasses the linking of the findings of this Paleosol to the evolution of the landscape and to the estimation of climate change impacts, besides this soil being rarely found in tropical regions, mainly considering their contrasting redoximorphic features, comprising the first Paleosol investigation via digital morphometrics under such conditions.

2. Material and methods

2.1. Soil location and sampling

The selected Paleosol, which was very difficult to access and sample, consists of a rare finding in Brazil that deserves this detailed characterization, constituting a pilot study. This Paleosol profile is located at the Pontal do Paranapanema region (Fig. 1), western São Paulo state, Brazil. It was classified as typic Dystrophic Tb Haplic Cambisol, following the Brazilian Soil Classification System (SiBCS) (Santos et al., 2015a; 2018), corresponding to Oxic Dystrustept per the US Soil Taxonomy (Soil Survey Staff, 2014), Dystric Rhodic Cambisol (Loamic, Ochric) per the World Reference Base (FAO, 2022), and Cambosol Ustic per Chinese Soil Taxonomy (CRG-CST, 2001), intermediary to a typic eutrophic Tb Haplic Gleysol (per SiBCS), Aeric Endoaquent (per US Soil Taxonomy), Eutric Gleysol (Loamic, Ochric) (per WRB), and Gleysol Orthic (per Chinese Soil Taxonomy).
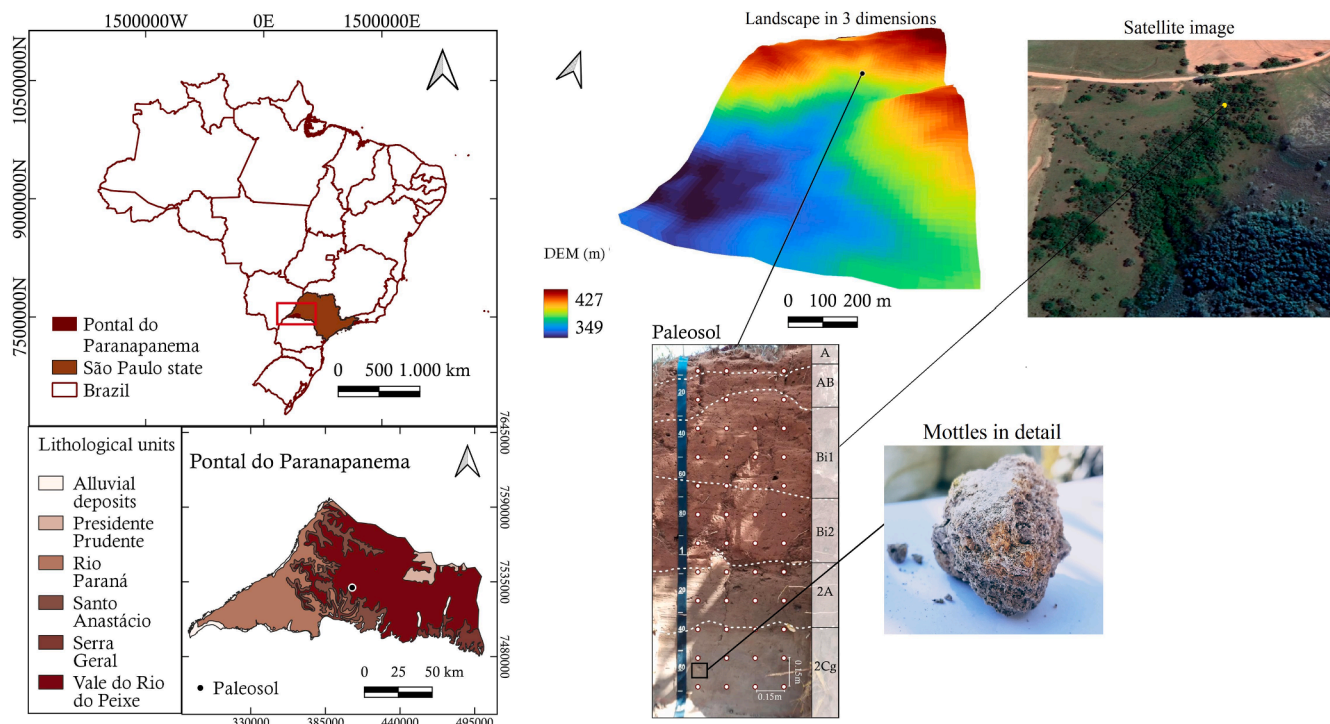

Fig. 1. Location of the Paleosol studied, sampling points within the profile, and regional lithological units from Pontal do Paranapanema region, São Paulo state, Brazil. Dashed lines represent the boundaries of the soil horizons delineated in the field.

The Paleosol is situated at the latitude 7,530,747 S and longitude 404,737 W, UTM, zone 22 K, *datum* SIRGAS 2000. It occupies the midslope position on a landscape with a gently undulated relief (7% slope). The climate of the region is Aw, framed as a tropical, in which the summer is rainy with average temperatures above 22 °C, and the winter is dry (Alvares et al., 2013). The soil profile was developed primarily from sandstone of the Bauru Group, Adamantina Formation, included in the Vale do Rio do Peixe lithological unit (Fig. 1). In such sandstones, mixture of pellitic sediments are common. These fine layers have much lower permeability than the sandstone. According to Stradioto and Chang (2020), this sandstone is mainly composed of quartz and feldspars and have micas and augite as the main accessory minerals. The native vegetation is represented by the semi-perennial tropical forest (Oliveira-Filho and Fontes, 2000).

2.2. Soil sampling and laboratory analyses

Soil samples were collected to 1.8 m of depth, on a regular grid design of 15x15 cm, comprising a total of 48 samples. This grid interval was adopted after evaluating the morphological features during the field work and based on the range of grid intervals found in the literature (Zhang and Hartemink, 2017; Sun et al., 2020, Mancini et al., 2023). Soil horizons were identified and morphologically described according to the Manual for Description and Sampling of Soil in the Field (Santos et al., 2015b).

Composite samples, obtained after careful mixing of four simple samples collected at each depth, were air-dried and gently sieved (2 mm) to obtain the air-dried fine earth (ADFE) fraction, and then submitted to the following chemical and physical analyses: pH in water, using a Digimed® (São Paulo, Brazil) pH-meter model DM-23-DC (Donagema et al., 2011), exchangeable contents of Ca^{2+}, Mg^{2+}, and Al^{3+} using a 1 mol/L KCl extraction solution (Mclean et al., 1958), available contents of K^+ and P using the Mehlich-1 extraction solution (Mehlich, 1953), H + Al using the SMP extractor (Shoemaker et al., 1961); soil organic matter (SOM) following Nelson and Sommers (1996), and using the van Bemmelen factor (1.724); remaining P (P-Rem) content, which refers to P content not adsorbed by soil organic and mineral particles (Alvarez et al., 2000) (all quantifications were performed via inductively coupled plasma optical emission spectroscopy, model Spectro Blue, Spectro Analytical Instruments, Germany); and particle size analysis by the pipette method (Gee and Bauder, 1986). The sand fraction was later separated into: very coarse (2–1 mm), coarse (1–0.5 mm), medium (0.5–0.25 mm), fine (0.25–0.105 mm), and very fine (<0.105 mm) sand, using dry sieving. Effective cation exchange capacity, cation exchange capacity at pH 7, sum of bases, base saturation, and Al^{3+} saturation were calculated based on the previous analyses.

2.2.1. Analyses via portable X-ray fluorescence (pXRF) spectrometry and magnetic susceptibility (MS) measurements

Twenty grams of ADFE of each collected sample (48 samples in total) were irradiated using a portable X-ray fluorescence (pXRF) spectrometer, Bruker® model Tracer 5g, connected to power line, containing a 50 keV and a 100 μA Rh X-ray tube using the "Soil" mode. The analyses were performed in triplicate, during 60 s each (Silva et al., 2021; Weindorf and Chakraborty, 2016). Then, the mean elemental contents of the triplicates per sample were calculated and used in further analyses. The calibration of the equipment was performed using a check sample (CS) provided by the manufacturer and two samples certified by the National Institute of Standards and Technology (NIST) (2710a and 2711a). The recovery values (Koch et al., 2017) (content reported by the pXRF/certified content × 100) were (2710a/2711a/CS): Al – 84/73/92; Ca – 39/45/–; Cr - –/107/–; Cu – 81/69/91; Fe – 71/65/88; K – 60/46/83 (41 mg/kg); Mg (–/65/–); Mn – 68/60/82; P (214/234/–); Si – 57/48/87; Ti – 77/65/–; V – 51/27/–; Zn – 87/82/– (3 mg/kg); Zr (85/–/–). The dashed lines indicate either no result by pXRF or no certified content

in the material.

For magnetic susceptibility (MS) measurements, 10 g of ADFE of each collected sample were analyzed in triplicate with a Bartington MS2B susceptibilimeter at low (LF) and high (HF) frequencies, according to Dearing (1999). The results are expressed on a mass-normalized basis, applying the following equation:

$$MS(\chi) = \chi_{LF} \ or \ \chi_{HF} result/sample \ weight \qquad (1)$$

where: MS = magnetic susceptibility ($\times 10^{-7}$ m^3 kg^{-1}); χ_{LF} and χ_{HF} result = result obtained for low and high frequency, respectively; and sample weight (g).

The difference of the results obtained at high and low frequencies (FD) was calculated per soil particle size fraction as follows:

$$FD\% = [(\chi_{LF} - \chi_{HF})\chi_{LF}] \times 100 \qquad (2)$$

These calculations contribute to the identification of ferrimagnetic minerals, since the reflection of the maghemite peaks in X-ray diffraction (XRD) analysis may coincide with the hematite peaks (Poggere et al., 2018).

2.2.2. X-ray diffraction (XRD) analysis

Samples of coarse sand, fine sand, silt, and clay fractions were gently macerated in an agate mortar to obtain homogeneous non-oriented powder 600 mg samples (Brindley and Brown, 1980), passed through a 0, 25 mm sieve. After that, they were analyzed with a Bruker D2 PHASER diffractometer, in which the irradiation varied from 4 to 52 °2θ at 0.02°2θ s^{-1}. This diffractometer is equipped with the LYNXEYE^{TM}, a practically instantaneous linear model, which uses the DIFFRAC. SUITE^{TM} software to obtain the XRD patterns. The results were interpreted with the help of tables prepared by Brindley and Brown (1980).

2.3. Spatial evaluation of the soil profile

The elemental contents determined via pXRF and the MS values were spatialized to the soil profile utilizing the multilevel B-spline method (Lee et al., 1997), within the software QGIS 3.22 (QGIS Development Team, 2022). This procedure contributes to better visualize the variation of such measurements along the soil profile, within and in between soil horizons (Hartemink et al., 2020).

3. Results and discussions

3.1. Soil morphology, fertility, texture and magnetic susceptibility analyses

By analyzing the soil profile in the field, it is noteworthy that two opposing processes occurred under different time periods. The first 108 cm of the profile is marked by oxidation conditions (favoring the formation of hematite that caused the red color of soil matrix), while redoximorphic conditions occurred in the 108–180 cm of the profile, producing greyish colors in the 2Cg horizon (Table 1). For the formation of hematite, oxidation conditions are required in combination with higher availability of Fe(III), favored by free drainage (Kämpf et al., 2012).

The soil underneath presents a 2A horizon (108–142 cm) (Table 1), followed by gleyzation features in the deeper portions of the profile. This part of the soil profile was probably formed on an ancient, gentler landscape, which was, later on, dissected by water erosion (Resende et al., 2021).

Given the greyish color of the lowest part of the soil profile (142–180 cm) (Table 1), below the 2A horizon, probably this soil occupied an area more gentle and prone to accumulation of water, favored by the pellitic sediments intermixed with the sandstone, causing the gleization process (Barbosa et al., 2019). The small red and red-yellow mottles observed in this soil horizon support the possibility of perched water table

Table 1

Synthetic morphological description of the studied soil profile from Pontal do Paranapanema, São Paulo state, Brazil.

Horizon	Depth (cm)	Soil Color* (moist)		Structure
A	0–12	2.5YR 3/2	Dusky red	Granular
AB	12–23	2.5YR 3/3	Dark reddish brown	Granular
Bi1	23–65	2.5YR 3/4	Dark reddish brown	Subangular blocky, which falls apart into granules
Bi2	65–108	2.5YR 3/6	Dark red	Subangular blocky, which falls apart into granules
2A	108–142	7.5YR 3/4	Dark brown	Granular
2Cg	142–180 cm+	10YR 5/2; 2.5YR 6/6 and 5YR 6/8 small mottles	Grayish brown; light red and reddish yellow	Massive

*Soil color by the Munsell Soil Color Chart.

oscillation (Kämpf and Curi, 2000). Interestingly, its actual location on the landscape (midslope position with 7% slope) does not favor water accumulation, indicating a probable change on the landscape from the time this unity was formed to the present day. Resende et al. (2019) stated that the landscape in Brazil has changed a lot as a function of intense water erosion. This erosion has been so effective that some strata of the geologic column, which are quite common in another parts of world, are absent in a substantial portion of Brazil.

Soil pH varied from 4.8 to 6.0, and the lower values were mainly found in the upper part of the soil profile (Table 2). This part has been submitted to weathering-leaching causing acidification, a common feature of most Brazilian soils (Resende et al., 2021). Conversely, the unity below presented greater contents of nutrients, highlighting the almost twice greater contents of exchangeable Ca^{2+} and Mg^{2+}, greater cation exchange capacity at pH 7, sum of bases, and pH values. Available P content was null in all depths evaluated, except for the first one, probably related to nutrient recycling by vegetation, although it was very low (0.02 mg dm^{-3}). Low or null contents of exchangeable Al^{3+} were found in all soil samples, probably related to its consumption during the formation of kaolinite, feldspars, and mica (see Fig. 5). The SOM content decreased from the A to Bi2 horizon and then sharply increased in the 2A horizon (from 0.35 to 0.89 dag kg^{-1}), corroborating the latter designation during the morphological description and sampling. This variation of SOM content serves as a registration of the alteration from a paleo-more gentle landscape, favoring water and, hence, SOM accumulation (confirmed by greater SOM contents), to a current more undulated landscape that prevents water accumulation,

decreasing the SOM contents found in the current surface of the profile.

The particle size distribution of the soil profile (Table 3) showed the highest sand contents in the deepest sample collected, where the fine sand fraction is predominant ($\sim$60 %). Also, the fine sand and silt contents are very different in various portions of the profile, indicating a possible variation of the soil parent material (Resende et al., 2014). While medium sand contents were homogenous in depth, the total sand fraction varied between the upper portion (from 61 to 79 %) and the lower portion of the soil profile (from 78 to 90 %). The clay contents ranged from 8.0 to 20 %; the highest contents occurred in the upper portion of the soil profile. More importantly, the clay content in the lower portion is considerably lower, reaching half of the lowest content (8 %) found in the upper portion of the soil profile (16 %). Silt contents were also divergent in the soil profile, varying from 1 % in the lower portion to 21 % in the upper portion. This fraction content is highest at the depth of 70 cm (21 %) and the lowest values are found in the lower portion of the soil profile. The silt/clay ratio being equal or higher than 0.7 in the Bi1 and Bi2 horizons excludes the classification of this soil as Latosol (Santos et al., 2015a; Santos et al., 2018), indicating this soil did not suffer a high degree of weathering.

The magnetic susceptibility (MS) analysis of A and Bi1 soil horizons indicated magnetic minerals in all the particle size fractions, with the greatest contents in the clay fraction (Table 4). In the clay fraction, the MS values doubled from the A to the Bi1 horizon, which may indicate some lateral loss of clay from the A horizon (Table 3) (Gonçalves et al., 2019), with possible removal of some maghemite.

In the coarse sand fraction of the A horizon, the same values for low and high frequencies of MS, with consequent null value of FD % (Table 4), indicate the presence of only macro-sized multidomain (MD) ferrimagnetic minerals of lithogenic origin in this soil fraction (Preetz et al., 2017). In the Bi1 horizon, the FD value of 12.2 % suggests the predominance of ultrafine-grained ferrimagnetic minerals formed during pedogenesis (super-paramagnetic – SP – minerals) (Preetz et al., 2017).

In the silt fraction of the A and Bi1 soil horizons, values of FD of 8.6 and 8.0 %, respectively, suggest similar proportions of MD and SP minerals, while in the clay fraction, the FD value of 15.3 % indicates substantial predominance of SP minerals. In the silt fraction of the 2A horizon, the FD value of 7.1 % suggests equilibrium between MD and SP minerals, while in the clay fraction the value of FD of 12.5 % indicates predominance of SP minerals.

In the coarse and fine sand fractions of 2A and 2Cg soil horizons, the MS values of 0 and 0.7x10^{-7} m^3 kg^{-1} indicate absence and only traces of magnetic minerals, respectively (Dearing, 1999). The much lower values of MS in the silt and clay fractions of the 2Cg soil horizon (Table 4) is in agreement with the paleoredoximorphic conditions prevailing there, causing destabilization and removal of magnetite from the silt fraction

Table 2

Results of soil fertility analyses of the studied soil profile, from Pontal do Paranapanema, São Paulo state, Brazil.

Depth	pH	K^+	P	Ca^{2+}	Mg^{2+}	Al^{3+}	H + Al	SB	t	T	BS	Al sat	SOM	P-Rem
cm		mg dm^{-3}					$cmol_c$ dm^{-3}					%	dag kg^{-1}	mg L^{-1}
0–10	5.2	70.03	0.02	0.76	0.35	0.0	1.8	1.29	1.29	3.09	41.73	0.00	0.73	50.8
10–25	4.8	63.77	0.00	0.65	0.27	0.1	3.6	1.08	1.18	4.68	23.15	8.47	0.43	44.8
25–40	5.2	61.92	0.00	0.67	0.36	0.1	1.7	1.19	1.29	2.89	41.13	7.75	0.39	42.3
40–55	5.3	57.04	0.00	0.97	0.28	0.0	1.6	1.40	1.40	3.00	46.54	0.00	0.42	43.1
55–70	5.5	59.9	0.00	0.79	0.19	0.1	1.6	1.13	1.23	2.73	41.52	8.13	0.53	50.3
70–85	5.4	57.25	0.00	0.84	0.21	0.0	2.8	1.20	1.20	4.00	29.92	0.00	0.40	49.0
85–100	5.4	56.59	0.00	0.99	0.23	0.0	1.4	1.37	1.37	2.77	49.28	0.00	0.35	52.4
100–115	5.2	64.99	0.00	1.84	0.5	0.0	1.9	2.51	2.51	4.41	56.84	0.00	0.89	46.9
115–130	5.5	63.80	0.00	1.82	0.64	0.0	2.4	2.62	2.62	5.02	52.26	0.00	0.85	50.9
130–145	5.9	61.28	0.00	1.33	0.52	0.0	1.3	2.01	2.01	3.31	60.64	0.00	0.33	59.9
145–160	6.0	78.92	0.00	1.32	0.53	0.0	1.3	2.05	2.05	3.35	61.26	0.00	0.32	63.3
160–175	5.1	60.96	0.00	1.30	0.46	0.0	2.2	1.92	1.92	4.12	46.51	0.00	0.27	44.8

SB: sum of bases; t: effective cation exchange capacity; T: cation exchange capacity at pH 7; BS: base saturation; Al sat: saturation by Al^{3+}; SOM: soil organic matter; and P-Rem: remaining P.

Table 3
Texture analyses of the studied soil profile, from Pontal do Paranapanema, São Paulo state, Brazil.

Depth	Clay	Silt	Very coarse sand	Coarse sand	Medium sand	Fine sand	Very fine sand	Total sand	Silt/clay ratio
cm						—%—			
0–10	17	9	0	0	6	51	17	74	0.55
10–25	19	2	0	1	6	55	17	79	0.12
25–40	19	17	0	1	6	37	20	65	0.89
40–55	20	14	0	2	6	37	21	66	0.73
55–70	18	21	0	0	6	35	20	61	1.20
70–85	16	13	0	0	6	41	24	71	0.78
85–100	15	15	0	0	6	40	24	71	1.01
100–115	16	7	0	0	6	45	26	78	0.43
115–130	15	5	0	0	6	50	24	81	0.32
130–145	10	1	0	2	6	58	23	89	0.08
145–160	8	2	0	1	6	60	23	90	0.21
160–175	9	1	0	2	6	60	22	90	0.08

and maghemite from the clay fraction of the Paleosol (Kämpf and Curi, 2000; Resende et al., 2011). This process is caused by the reduction of Fe(III) to Fe(II) under reduction conditions (waterlogging preventing appropriate amounts of oxygen in soil pores), dismantling Fe(III)-bearing minerals, such as the magnetic ones (magnetite and maghemite), besides hematite and goethite (Kämpf and Curi, 2000; Schaetzl and Anderson, 2005); thus, it provides the greyish color and the low MS values of the 2Cg horizon.

The spatialization of MS data (Fig. 2) showed variation across the soil profile (the data presented in Figs. 2, 3 and 4 to be discussed later, may assist in horizons recognition and boundaries definition). The higher MS values were found in the Bi horizon. Probably the lower MS values in the A horizon are related to the greater content of SOM, which tends to reduce MS. Dearing (1999) classified the SOM as diamagnetic, presenting a weak or even negative susceptibility, reducing the final MS value of matrices presenting higher SOM contents. Moreover, the lowest MS values were found at 115–175 cm depth, indicating that this portion of the soil profile has the lowest contents of magnetic minerals, corroborating the hypothesis that it was formed under paleoredoximorfic conditions. As such, these conditions tend to destabilize the magnetic minerals, by reducing the Fe(III) to Fe(II) forms (Kämpf and Curi, 2000), with consequent removal. Shirzaditabar and Heck (2021), studying soils with different drainage conditions, found lower MS values for hydromorphic soils and higher values for well-drained soils, similar to the findings for the Gleysol and the Cambisol unities of the soil profile studied herein. There is a small part of the 2A horizon at its right superior side with contrasting much higher FD % values (Fig. 2), which may indicate that this part is more related to the Bi1 horizon situated above. It was not observed any indication of such difference during the field morphological analysis.

When comparing the MS values of ADFE, the lowest values were found for the 2Cg horizon, probably related to the instability of the magnetic minerals under paleoredoximorphic conditions (Kämpf and Curi, 2000; Resende et al., 2011). The increase of low and high frequency values of MS for the A to the Bi1 soil horizons reinforces the indication of lateral loss of clay from the A horizon (Gonçalves et al., 2019), with removal of some magnetite and maghemite.

3.2. Portable X-ray fluorescence (pXRF) and X-ray diffraction (XRD) analyses

The variation of the elemental contents detected by pXRF in the soil profile (Fig. 3) shows that some elements have a clear pattern of distribution. For instance, K increased downwards, starting from 115 cm of depth, coinciding with the 2A horizon of the soil. This increment is not associated with increasing available K content (Table 2), probably because K constitutes part of the crystalline structure of feldspars and mica (Fig. 5). The P and Zn had low variations along the soil profile,

presenting low contents. The Ca, Mg, and Si contents decreased until a certain depth (Ca and Mg between 85–100 cm and Si at ~ 55 cm) and then increased again. Different from K, Ca and Mg contents increased in depth in accordance to the increase of their exchangeable forms. The correlations between Ca, Mg, and K from pXRF and their exchangeable/available contents agree with reports from other studies conducted in Brazilian soils (Benedet et al., 2021; Silva et al., 2018; Teixeira et al., 2018).

The Cr, Cu, Fe, Mn, Ti, V, and Zr have higher contents in the upper part of the soil profile (A and Bi horizons) and lower contents below that depth (Fig. 4). Gloaguen and Passe (2017) studied the natural accumulation of Cr, Cu, Pb, Ni, and Zn in different soils derived from Quaternary sediments and in sandy soils derived from Mesozoic rocks, at Recôncavo Baiano region, Brazil, and concluded that the pedogenesis and the geology explain the concentration of such elements in these soils, similar to the present study.

The sandstone parent material influences the elemental content of the soil (Moniz and Carvalho, 1973), as expected. Heavy metals tend to accumulate mainly in the clay fraction of soils (Pikuła and Stepień, 2021). In the present study, greater content of elements was found in horizons featuring higher clay content (Fig. 3 and Table 3). The Fe content, for instance, revealed a drastic reduction from 145 cm depth downwards, corresponding to the portion of the soil where paleogleization processes prevailed (2Cg horizon), promoting the solubilization of Fe(II) forms and consequent removal by leaching.

The Ti/Zr ratio showed values of 21.45, 21.00, 39.74, and 34.00, respectively, for the A, Bi1, 2A, and 2Cg horizons, clearly indicating different parent materials for the Cambisol and Gleysol unities, since both elements are known as very stable and immobile in soil enviroments (Gozükara et al., 2021; McNulty et al., 2018; Schaetzl and Anderson, 2005; Stockmann et al., 2016). One possible explanation for such differences in parent materials refers to the well-known association of pellitic sediments intermixed with sandstone (Resende et al., 2019). The current midslope position of the Paleosol studied with 7% slope make the colluvia possibility unlikely.

Regarding the spatialization of elemental contents (Fig. 4), the distribution of several elements followed the occurrence of the different unities of the Paleosol. Noticeable, Al, Cr, Cu, Fe, Ti, V, Zn, and Zr accumulated in the Bi horizon and were lower downwards. The opposite trend occurred for Si and K. However, Mn clearly accumulated in the 2A horizon, reinforcing the occurrence of different soil parent materials. The accumulation of Al, Cr, Cu, Fe, Ti, V, Zn, and Zr in the Bi horizons is associated with their greater clay content (Table 3). Mancini et al. (2021) and Sun et al. (2020) also observed that some elements accumulated in the B horizon, respectively, of a Latosol (Oxisol) and an Alfisol, coincident with relative greater accumulation of clay in such horizons of the soil profiles.

Regarding the XRD analyses (Fig. 5), quartz predominates in the silt,

Table 4

Magnetic susceptibility (χ) in low frequency (χ_{LF}), high frequency (χ_{HF}), and the frequency difference (FD) per granulometric fraction and for the air-dried fine earth (ADFE) fraction of the studied profile, from Pontal do Paranapanema, São Paulo state, Brazil.

χ	Horizon	Coarse sand	Fine sand	Silt	Clay	ADFE
χ_{LF}	A	8.6	5.2	3.9	52.4	10.1
	Bi1	5.6	1.9	15.3	104.7	20.5
	2A	0.0	0.7	16.9	35.0	6.2
$(\times 10^{-7} \text{ m}^3 \text{ kg}^{-1})$	2Cg	0.0	0.7	3.9	4.8	1.3
χ_{HF}	A	8.6	4.7	3.6	44.4	9.0
	Bi1	4.9	1.6	14.1	88.6	17.7
	2A	0.0	0.7	15.7	30.3	5.6
$(\times 10^{-7} \text{ m}^3 \text{ kg}^{-1})$	2Cg	0.0	0.7	3.9	4.2	1.2
χ_{FD}	A	0.0	0.5	0.3	8.0	1.1
(χ_{LF} - χ_{HF})	Bi1	0.7	0.3	1.2	16.0	2.8
	2A	0.0	0.0	1.2	4.7	0.6
$(\times 10^{-7} \text{ m}^3 \text{ kg}^{-1})$	2Cg	0.0	0.0	0.0	0.6	0.1
FD	A	0.0	9.1	8.6	15.3	10.9
(%)	Bi1	12.2	17.6	8.0	15.3	13.7
	2A	0.0	0.0	7.1	13.5	9.7
	2Cg	0.0	0.0	0.0	12.5	8.3

coarse and fine sand fractions of all soil horizons. Small peaks of feldspars (probably K-feldspars) were identified in the coarse and fine sand fractions of 2A and 2Cg horizons (Fig. 5b; 5c; 5d). Moreover, mica was identified in the silt (probably muscovite) and clay (probably illite) fractions of the 2Cg horizon (Fig. 5d). Both findings help explain the increment of K obtained via pXRF in these soil horizons (Fig. 4), and agree with reports of Moniz and Carvalho (1973) when studying soils of the same region and derived from the same parent material.

In the clay fraction, kaolinite was the dominant mineral in all soil horizons, mainly in the 2Cg horizon. Hematite was not identified only in this horizon, as expected, since the paleoredoximorphic conditions probably caused its decomposition (Barbosa et al., 2019; Kämpf and Curi, 2000; Resende et al., 2011).

A small gibbsite peak was found only in the clay fraction of the 2Cg horizon (Fig. 5d), which is in agreement with the findings of Motta and Kämpf (1992) and Pozza et al. (2007, 2009) when studying a Haplic Gleysol profile in the Central Plateau of Brazil. Rutile was only detected in the silt and clay fractions of the 2Cg horizon. Taking into account this Ti-bearing mineral is very stable and immobile in soil systems, even under redoximorphic conditions (Kämpf et al., 2009), this finding may also corroborate the lithological discontinuity possibility discussed earlier.

According to pXRF results per particle size fraction of the soil (Fig. 6), Al is predominant in the clay fraction of all soil horizons. The same trend occurs for P, Zn, Ti, Cu, Cr, Fe, and V (except for the 2A horizon, which contains greater V content in the silt fraction). Conversely, Zr and Mn contents are predominant in the silt fraction, except for the 2Cg horizon that has higher contents of Mn in the clay fraction. Grauer-Gray and Hartemink (2018) found higher contents of Zr for soils richer in clay or silt (Alfisol and Mollisol) and lower contents for sandy soil (Entisol). Silva et al. (2018) also observed this trend for both Zr and Mn, mainly in the Cr horizon of a Cambison (Inceptisol) in the Brazilian Cerrado biome.

Nevertheless, Si, Mg, and Ca were well distributed along the soil profile in all soil fractions. The Si distribution is mainly associated to the dominance of quartz in the sand and silt fractions, and to kaolinite in the clay fraction of the soil studied.

4. Final remarks

The combination of analyses used in this pilot work was able to detail the contrasting pedogenesis processes of the Cambisol and Gleysol unities of the studied soil profile, confirming the field morphological description, in addition to revealing differences in parent materials, not-detected during the field work. The digital morphometrics approach, mainly in terms of magnetic susceptibility data spatialization, elucidated a clear variation in the boundaries between the Bi2 and 2A soil horizons, without any indication in field morphology.

The drain head where the Paleosol is situated (Fig. 1) is environmentally important mainly in relation to springs protection, because its conformation tends to expose the perched water table. So, it is important
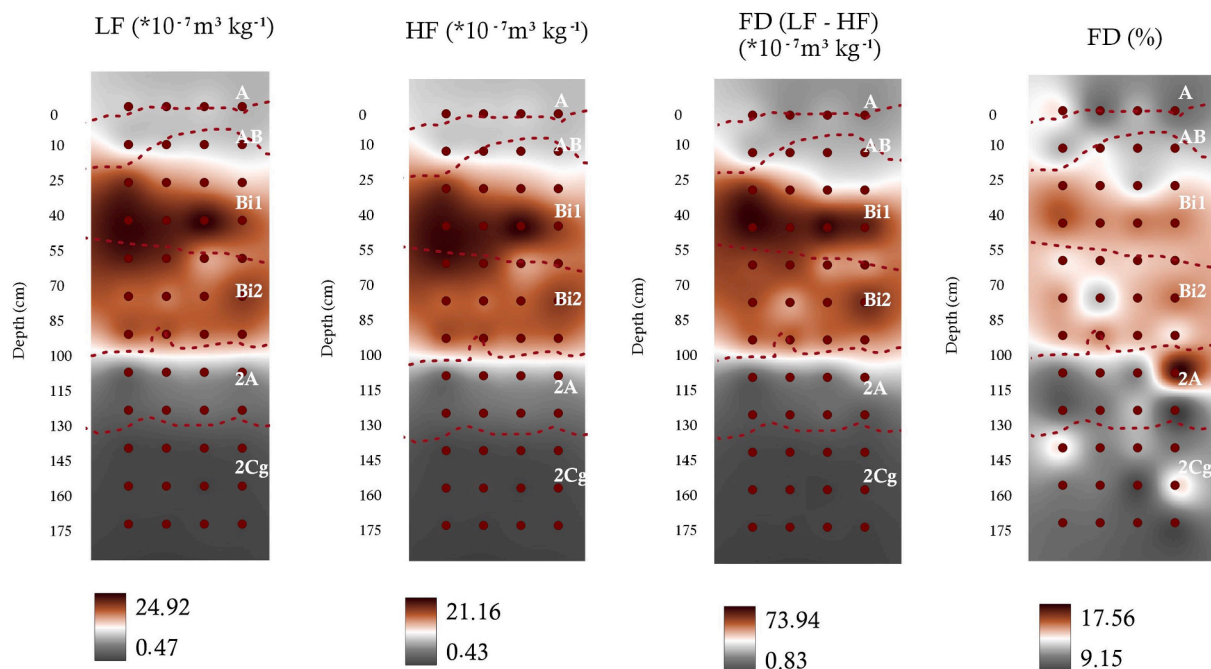

Fig. 2. Spatial representation of magnetic susceptibility data in low frequency (LF), high frequency (HF), and the frequency difference (FD) of the studied soil profile from Pontal do Paranapanema, São Paulo state, Brazil.
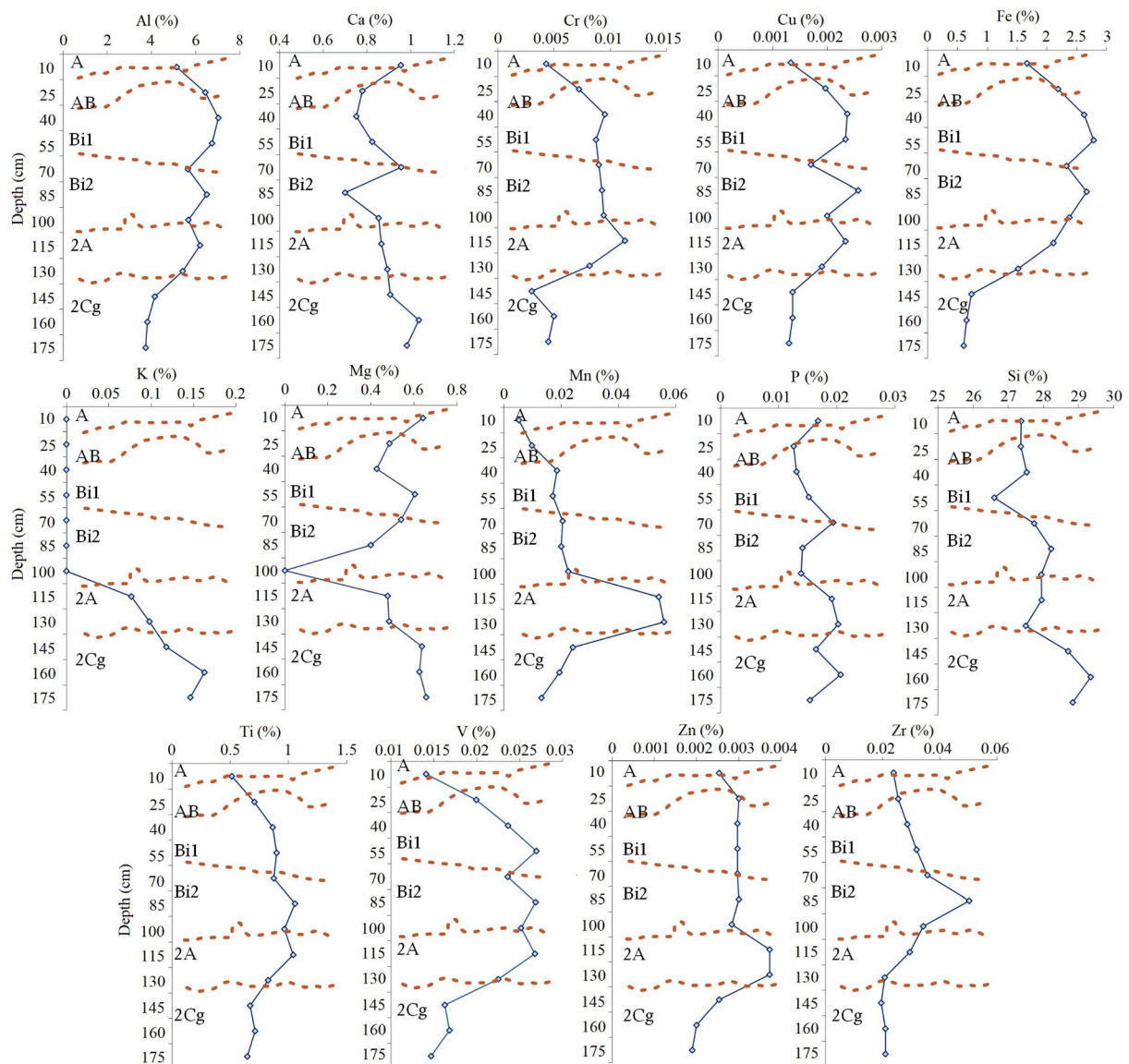
Fig. 3. Mean elemental contents of the studied soil profile, obtained with pXRF, from Pontal do Paranapanema, São Paulo state, Brazil. Dashed lines indicate horizon boundaries, established during field morphological description.

to detail the characterization of the soils there in order to plan conservation practices aiming to prevent the clogging of springs (Mello et al., 2019). As the sediments tend to remain retained on the native vegetation (semi-perennial tropical forest) of these areas, they play a role as filters, with beneficial impacts on water quality (Mello and Curi, 2012). The undulated topography of this drain head does not allow much impact on water recharge potential. Also, the seepage erosion should also be considered, in which the subsurface flow, favored in this case by the pellitic (fine) sediments intermixed with the sandstone, may transport soil particles entrained in the seepage water (Soil Science Society of America, 2008) to lower landscape positions and may potentially pollute water bodies and springs (Mello et al., 2019), mainly in terms of heavy metals, N, and P.

The detailed characterization of the Paleosol may be useful for estimation of water and sediment paleodischarge and paleodrainage area, and sediment budgets (Bhattacharya et al., 2016) and for paleodischarge reconstruction (Shen et al., 2021), then assisting with characterization of climate change impacts.

The authors understand that there are Paleosols not yet studied in Brazil, for example the Latosols (Oxisols) located on the summits

(*chapadas*) of the Brazilian Central Plateau, making part of the Cerrado biome (22% of the county). These *chapadas* were formed by pediplanation, under bioclimatic conditions much drier than nowadays (Curi et al., 1993). In other words, the relief is relict from dry climate and the Oxisols were formed under humid climate (Resende et al., 2014). Then, these Latosols are polygenetic: they are Paleosols. This approach may encourage future studies in this research line.

5. Conclusions

The Paleosol studied herein presented contrasting redoximorphic features, suggesting a change on the landscape to promote such variation. Moreover, the Ti/Zr ratio, delivered by pXRF, indicated different parent materials forming the reddish and gleyic unities of the Paleosol.

The topographical evolution includes a gentler slope in the past, allowing a high perched water table, favored by the pellitic (fine) sediments intermixed with the sandstone. These fine layers, having much lower permeability, induced paleoredoximorphic processes and the resulting greyish colors in the lower part of the Paleosol profile. After that, there was an intense erosion resumption, a very common condition
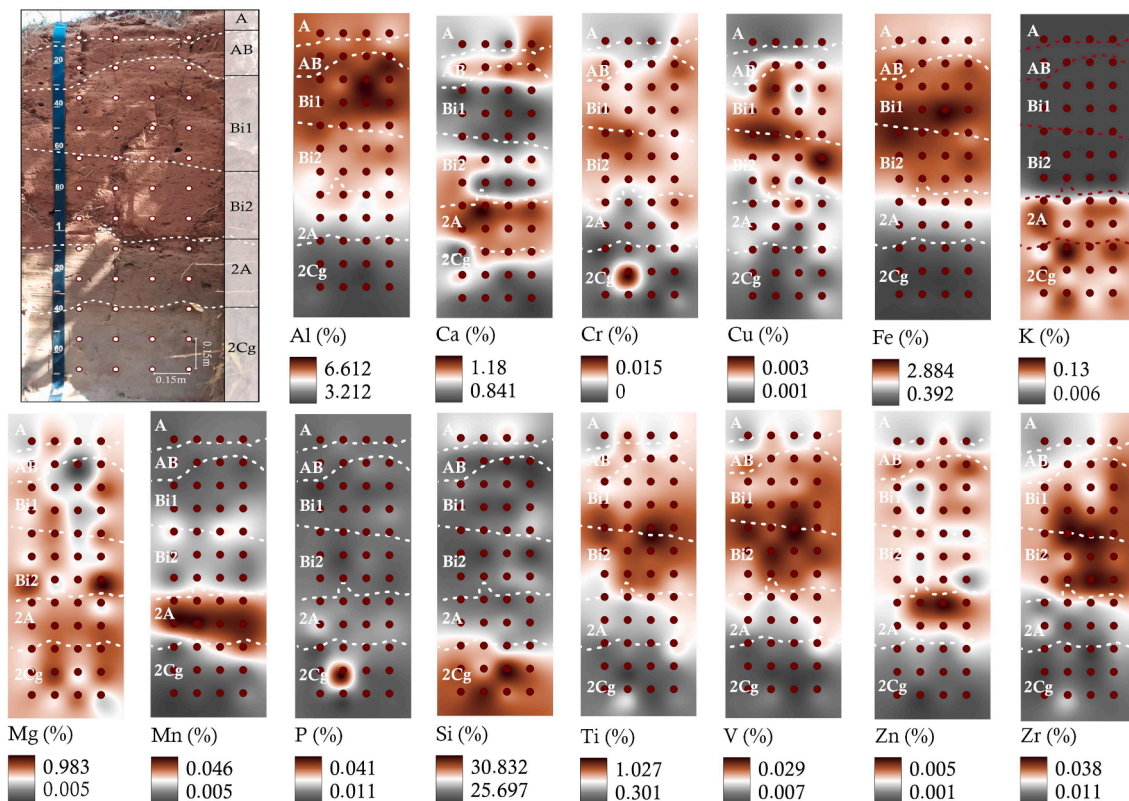
Fig. 4. Spatial representation of elemental contents variability of the studied profile, obtained with pXRF, from Pontal do Paranapanema, São Paulo state, Brazil.
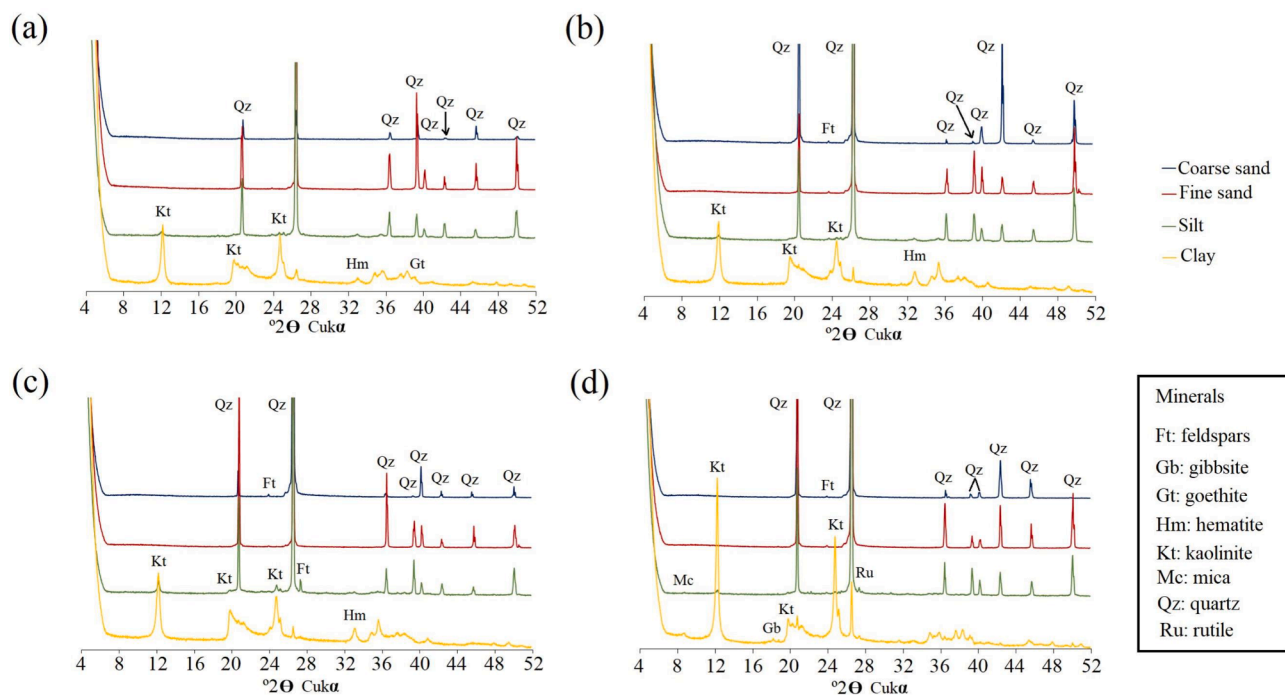

Fig. 5. X-ray diffraction analyses of particle size fractions of the soil studied, in Pontal do Paranapanema, São Paulo state, Brazil. **(a)** A horizon; **(b)** Bi1 horizon; **(c)** 2A horizon; and **(d)** 2Cg horizon.

in Brazil, dissecting the former landscape and favoring the current oxidation processes in the upper part of the soil profile, with hematite formation and consequent reddish colors.

In this pilot study, the combined use of field morphology, physical, chemical, and mineralogical analyses, complemented by pXRF and MS data, provided details on the variation of soil properties formed under current pedalization and elutriation versus paleogleyzation, and delivered some insights on enhancing conservation practices and on assisting the characterization of climate change impacts.
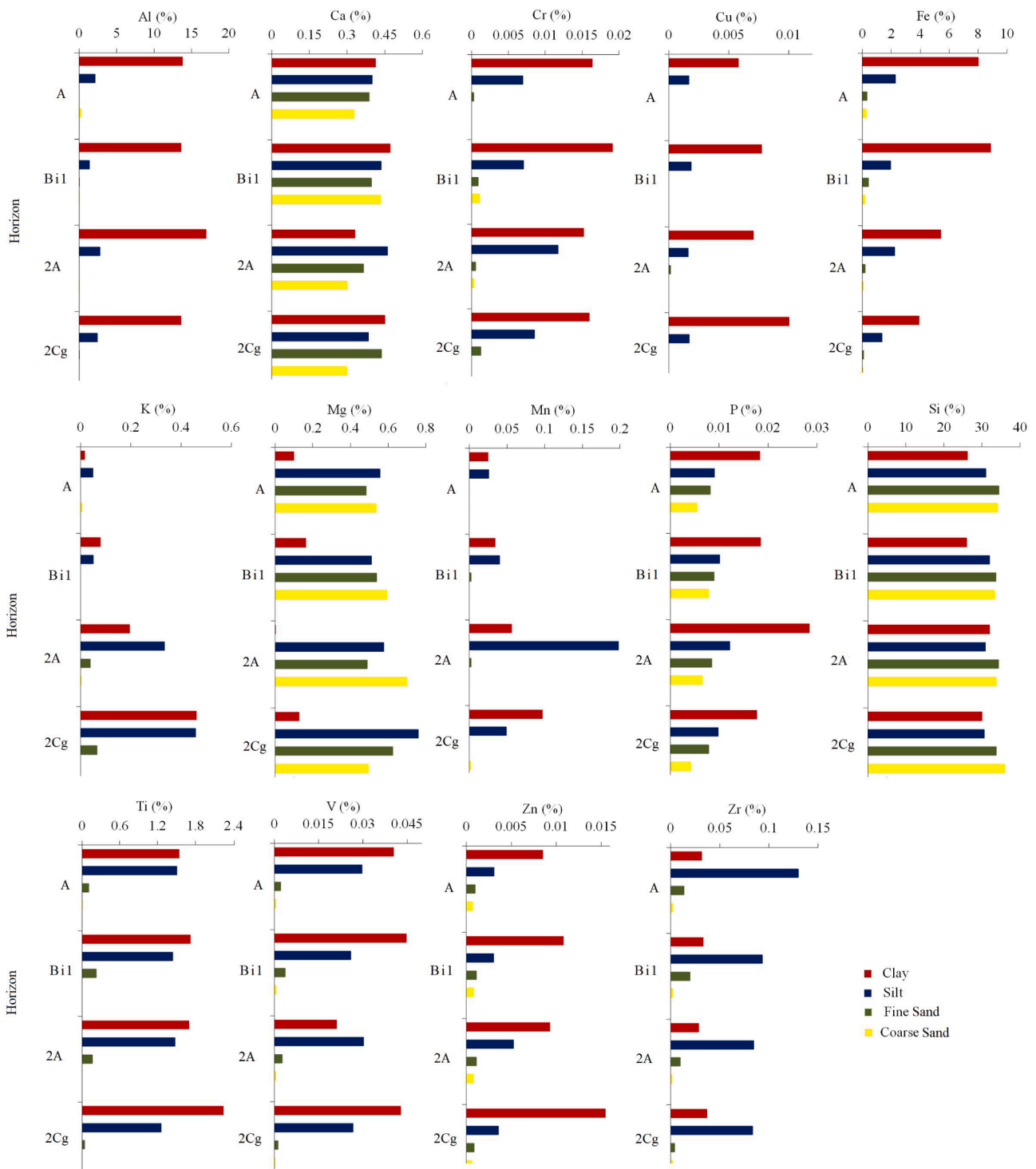
Fig. 6. Elemental contents per particle size fraction of the studied profile, obtained with pXRF, from Pontal do Paranapanema, São Paulo state, Brazil.

Declaration of Competing Interest

The authors declare the following financial interests/personal relationships which may be considered as potential competing interests: the authors report financial support was provided by Coordination of Higher Education Personnel Improvement, by National Council for Scientific and Technological Development, and by Minas Gerais State Foundation of Support to the Research.].

Data availability

Data will be made available on request.

References

Alvares, C.A., Stape, J.L., Sentelhas, P.C., de Moraes Gonçalves, J.L., Sparovek, G., 2013. Köppen's climate classification map for Brazil. Meteorol. Z. 22 (6), 711–728.

Alvarez, V.V.H., Novais, R.F., Dias, L.E., Oliveira, J.A., 2000. Determinação e uso do fósforo remanescente. Bol. Informativo da SBCS. 25, 27–32.

Barbosa, G.S., Maltoni, K.L., Panosso, A.R., 2019. The colors of soil as a parameter to delimitate the environment of a Palm Swampy. Bol. Goiano de Geografia, Goiânia. 39, 1–25. https://doi.org/10.5216/bgg.v39i0.52021.

Benedet, L., Acuña-Guzman, S.F., Faria, W.M., Silva, S.H.G., Mancini, M., Teixeira, A.F. S., Pierangeli, L.M.P., Acerbi Júnior, F.W., Gomide, L.R., Pádua Júnior, A.L., Souza, I.A., Menezes, M.D., Marques, J.J., Guilherme, L.R.G., Curi, N., 2021. Rapid soil fertility prediction using X-ray fluorescence data and machine learning algorithms. Catena 197, 105003. https://doi.org/10.1016/j.catena.2020.105003.

Bócoli, F.A., Silva, S.H.G., Mancini, M., Inda, A.V., Teixeira, A.F.S., Andrade, R., Silva, F. M., Santos, W.J.R., Pádua, E.J., Curi, N., 2023. Catena of Ultisols from southeastern Brazil: assessing variation within and among pedons. Geoderma Reg. 33, e00653.

Brindley, G.W., Brown, G., 1980. Crystal Structures of Clay Minerals and their X-ray Identification, 1st ed. Mineralogical Soc. of Great Britain and Ireland, London.

CRG-CST (Cooperative Research Group of Chinese Soil Taxonomy). 2001. Chinese Soil Taxonomy. Beijing, Science Press.

Curi, N., Kämpf, N., Resende, M., 1984. Mineralogia, química, morfologia e geomorfologia de solos originados de rochas efusivas das Encostas Superior e Inferior do Nordeste, no Rio Grande do Sul. Revista Brasileira de Cienc. do Solo. 8, 269–276.

Curi, N., Larach, J.O.I., Kämpf, N., Moniz, A.C., Fontes, L.E.F., 1993. Vocabulário de Ciência do Solo. SBCS.

Dearing, J., 1999. Environmental Magnetic Susceptibility: Using the Bartington MS2 system, 2nd ed. Kenilworth, Chi Publishing.

Donagema, G.K., Campos, D.V.B., Calderano, S.B., Teixeira, W.G., Viana, J.H.M., 2011. Manual de Métodos de Análise de Solo, 2nd ed. Embrapa Solos, Rio de Janeiro.

FAO, 2022. World reference base for soil resources/ International soil classification system for naming soils and creating legends for soil maps, 4th ed. FAO, Rome.

Gee, G.W., Bauder, J.W., 1986. Particle-size analysis. In: Klute, A. (Ed.), Methods of Soil Analysis. Am. Soc. of Agronomy, Madison, pp. 383–412.

Gloaguen, T.V., Passe, J.J., 2017. Importance of lithology in defining natural background concentrations of Cr, Cu, Ni, Pb and Zn in sedimentary soils, northeastern Brazil. Chemosphere 186, 31–42. https://doi.org/10.1016/j.chemosphere.2017.07.134.

Gonçalves, M.G.M., Ker, J.C., Oliveira, F.S., Ramos, L.O.S., Pacheco, A.A., Curi, N., 2019. Lateral loss of clay in the genesis of Luvisols in the Semi-Arid Depression of the Jequitinhonha Valley, Minas Gerais - Brazil. Cienc. e Agrotecnologia. 43, e018219.

Gozukara, G., Zhang, Y., Hartemink, A.E., 2021. Using vis-NIR and pXRF data to distinguish soil parent materials – An example using 136 pedons from Wisconsin, USA. Geoderma 396, 115091. https://doi.org/10.1016/j.geoderma.2021.115091.

Grauer-Gray, J., Hartemink, A.E., 2018. Raster sampling of soil profiles. Geoderma 318, 99–108. https://doi.org/10.1016/j.geoderma.2017.12.029.

Hartemink, A.E., Minasny, B., 2014. Towards digital soil morphometrics. Geoderma 230–231, 305–317. https://doi.org/10.1016/j.geoderma.2014.03.008.

Hartemink, A.E., Zhang, Y., Bockheim, J.G., Curi, N., Silva, S.H.G., Grauer-Gray, J., Lowe, D.J., Krasilnikov, P., 2020. Soil horizon variation: a review. Adv. Agron. 160, 125–185. https://doi.org/10.1016/bs.agron.2019.10.003.

Jenny, H., 1941. Factors of soil formation: A system of quantitative Pedology. McGraw-Hill, Book Co., Inc, New York.

Kämpf, N., & Curi, N. 2000. Óxidos de ferro - Indicadores de atributos e ambientes pedogenênicos e geoquímicos. In R. F. NOVAIS, V. V. H. ALVAREZ, & C. E. G. R. SCHAEFER (Eds.), Tópicos em Ciência do Solo (pp. 107–138). Sociedade Brasileira de Ciência do Solo.

Kämpf, N., Curi, N., & Marques, J. J. (2009). Óxidos de alumínio, silício, manganês e titânio. In V. F. Melo & L. R. F. Alleoni (Eds.), Química e mineralogia do solo (1st ed.). SBCS.

Kämpf, N., Marques, J.J., Curi, N., 2012. Mineralogia de Solos Brasileiros: Principais Aspectos. In: Ker, J.C., Curi, N., Schaefer, C.E.G.R., Vidal-Torrado, P. (Eds.), Pedologia: Fundamentos. SBCS, Viçosa, pp. 80–145.

Koch, J., Chakraborty, S., Li, B., Kucera, J.M., Van Deventer, P., Daniell, A., Faul, C., Man, T., Pearson, D., Duda, B., Weindorf, C.A., Weindorf, D.C., 2017. Proximal sensor analysis of mine tailings in South Africa: An exploratory study. J. Geochemical Explor. 181, 45–57. https://doi.org/10.1016/j.gexplo.2017.06.020.

Ladeira, F.S.B., 2010. Soils of the Past: Origin and Identity. Revista Brasileira de Cienc. do Solo. 34, 1773–1786. https://doi.org/10.1590/S0100-06832010000600001.

Lee, S., Wolberg, G., Shin, S.Y., 1997. Scattered Data Interpolation with Multilevel B-Splines. IEEE Trans. Vis. Comput. Graph. 3, 228–244. https://doi.org/10.1109/2945.620490.

Mancini, M., Silva, S.H.G., Hartemink, A.E., Zhang, Y., Faria, Á.J.G., Silva, F.M., Inda, A. V., Demattê, J.A.M., Curi, N., 2021. Formation and variation of a 4.5 m deep Oxisol in southeastern Brazil. Catena 206, 105492. https://doi.org/10.1016/j.catena.2021.105492.

Mancini, M., Silva, S.H.G., Avanzi, J.C., Hartemink, A.E., Inda, A.V., Demattê, J.A.M., de Lima, W., Curi, N., 2023. Digital morphometrics and genesis of soils with buried horizons and lithological discontinuities in southeastern Brazil. Geoderma Reg. 32, e00612.

Mclean, E.O., Heddleson, M.R., Bartlett, R.J., Holowaychuk, N., 1958. Aluminum in soils: I. Extraction methods and magnitudes in clays and Ohio soils 1. Soil Sci. Soc. of Am. Journal. 22, 382–387. https://doi.org/10.2136/sssaj1958.03615995002200050005x.

McNulty, B.A., Fox, N., Berry, R.F., Gemmell, J.B., 2018. Lithological discrimination of altered volcanic rocks based on systematic portable X-ray fluorescence analysis of drill core at the Myra Falls VHMS deposit. Canada. J. Geochemical Explor. 193, 1–21. https://doi.org/10.1016/j.gexplo.2018.06.005.

Mehlich, A., 1953. Determination of P, Ca, Mg, K, Na and NH$_4$. North Carolina Soil Testing Division, Raleigh, NC.

Mello, C.R.d., Curi, N., 2012. Hydropedology. Hydropedology. Ciência e Agrotecnologia 36 (2), 137–146.

Mello, D.C., Demattê, J.A.M., Silvero, N.E.Q., Raimo, L.A.D.L., Poppiel, R.R., Mello, F.A. O., Souza, A.B., Safanelli, J.L., Resende, M.E.B., Rizzo, R., 2020. Soil magnetic susceptibility and its relationship with naturally occurring processes and soil attributes in pedosphere, in a tropical environment. Geoderma 372, 114364. https://doi.org/10.1016/j.geoderma.2020.114364.

Mello, C.R., Norton, L.D., Pinto, L.C., Curi, N., 2019. Hydropedology in the tropics, 1st ed. Editora UFLA, Lavras.

Moniz, A.C., Carvalho, A., 1973. Sequência de evolução de solos derivados do arenito Bauru e de rochas básicas da região noroeste do estado de São Paulo. Bragantia 32, 309–335. https://doi.org/10.1590/s0006-87051973000100017.

Motta, P.E.F., Kämpg, N., 1992. Iron oxide properties as support to soil morphological features for prediction of moisture regimes in Oxisols of Central Brazil. Pflanzenernahr. Bodenk. 155, 385–390.

Nascimento, D.L., Ladeira, F.S.B., Batezelli, A., 2017. Pedodiagenetic Characterization of Cretaceous Paleosols in Southwest Minas Gerais, Brazil. Revista Brasileira de Cienc. do Solo. 41, e0160065.

Nelson, D.W., Sommers, L., 1996. Total carbon, organic carbon, and organic matter: Chemical methods. In: Black, C.A. (Ed.), Methods of Soil Analysis, Part 3. Soil Science of America and American Society of Agronomy, Madison, pp. 961–1010.

Oliveira-Filho, A., Fontes, M., 2000. Patterns of Floristic Differentiation among Atlantic Forests in Southeastern Brazil and the Influence of Climate. Biotropica 32, 793–810. https://doi.org/10.1111/j.1744-7429.2000.tb00619.x.

Phillips, J.D., 2016. Identifying sources of soil landscape complexity with spatial adjacency graphs. Geoderma 267, 58–64. https://doi.org/10.1016/j.geoderma.2015.12.019.

Pikuła, D., Stępień, W., 2021. Effect of the Degree of Soil Contamination with Heavy Metals on Their Mobility in the Soil Profile in a Microplot Experiment. Agronomy 11, 878. https://doi.org/10.3390/agronomy11050878.

Poggere, G.C., Inda, A.V., Barrón, V., Kämpf, N., Brito, A.D.B., Barbosa, J.Z., Curi, N., 2018. Maghemite quantification and magnetic signature of Brazilian soils with contrasting parent materials. Appl. Clay Sci. 161, 385–394. https://doi.org/10.1016/j.clay.2018.05.014.

Pozza, A.A.A., Curi, N., Costa, E.T.S., Guilherme, L.R.G., Marques, J.J.G.S.M., Motta, P.E. F., 2007. Retenção e dessorção competitivas de ânions inorgânicos em gibbsita natural de solo. Pesq. Agropec. Bras. 42, 1627–1633.

Pozza, A.A.A., Curi, N., Guilherme, L.R.G., Marques, J.J.G.S.M., Costa, E.T.S., Zuliani, D. Q., Motta, P.E.F., Martins, R.S., Oliveira, L.C.A., 2009. Adsorção e dessorção aniônicas individuais por gibbsita pedogenética. Quim Nova 32, 99–105.

Preetz, H., Igel, J., Hannam, J.A., Stadler, S., 2017. Relationship between magnetic properties and reddening of tropical soils as indicators of weathering. Geoderma 303, 143–149. https://doi.org/10.1016/j.geoderma.2017.05.007.

QGIS Development Team, 2022. QGIS Geographic Information System. Open-Source Geospatial Foundation. https://qgis.org/en/site/.

Resende, M., Curi, N., Ker, J.C., Rezende, S.B., 2011. Mineralogia de solos brasileiros - Interpretações e aplicações, (2nd ed.). Editora UFLA.

Resende, M., Curi, N., Rezende, S.B., Corrêa, G.F., Ker, J.C., 2014. Pedologia: Base para distinção de ambientes, 6th ed. Editora UFLA, Lavras.

Resende, M., Curi, N., Rezende, S.B., Silva, S.H.G., 2019. Da rocha ao solo: Enfoque ambiental, 1st ed. Editora UFLA, Lavras.

Resende, M., Curi, N., Poggere, G.C., Barbosa, J.Z., Pozza, A.A.A., Teixeira, A.F.S., 2021. Pedologia, fertilidade, água e planta: Inter-relações e aplicações, 2nd ed. Editora UFLA, Lavras.

Santos, R.D., Curi, N., Shimizu, S.H., 2015a. Guia prático para classificação de solos brasileiros. Editora UFLA, Lavras.

Santos, H.G., Jacomine, P.K.T., Anjos, L.H.C., Oliveira, V.A., Lumbreras, J.F., Coelho, M. R., Almeida, J.A., Araújo Filho, J.C., Oliveira, J.B., Cunha, T.J.F., 2018. Sistema Brasileiro de Classificação de Solos, 5th ed. Embrapa Solos, Brasília.

Santos, R.D., Santos, H.G., Ker, J.C., Anjos, L.H.C., Shimizu, S.H., 2015b. Manual de descrição e coleta de solo no campo, 7th ed. SBCS, Viçosa.

Schaetzl, R., Anderson, S., 2005. Soils: Genesis and geomorphology, (1st ed.). Cambridge University Press.

Shirzaditabar, F., Heck, R.J., 2021. Characterization of soil drainage using electromagnetic induction measurement of soil magnetic susceptibility. Catena 207, 105671. https://doi.org/10.1016/j.catena.2021.105671.

Shoemaker, H.E., Mclean, E.O., Pratt, P.F., 1961. Buffer methods for determining lime requirement of soils with appreciable amounts of extractable aluminum. Soil Sci. Soc. of Am. Journal. 25, 274–277. https://doi.org/10.2136/sssaj1961.03615995002500040014x.

Silva, M.L., Batezelli, A., Ladeira, F.S.B., 2017. The mineralogy of paleosols in the Marília Formation and their importance in the environmental evolution of the Maastrichtian of the Bauru Basin in southeastern Brazil. Braz. J. Geol. 47, 403–426. https://doi.org/10.1590/2317-4889201720170101.

Silva, S.H.G., Hartemink, A.E., Teixeira, A.F.S., Inda, A.V., Guilherme, L.R.G., Curi, N., 2018. Soil weathering analysis using a portable X-ray fluorescence (pXRF)

spectrometer in an Inceptisol from the Brazilian Cerrado. Appl. Clay Sci. 162, 27–37. https://doi.org/10.1016/j.clay. 2018.05.028.

Silva, S.H.G., Ribeiro, B.T., Guerra, M.B.B., Carvalho, H.W.P., Lopes, G., Carvalho, G.S., Guilherme, L.R.G., Resende, M., Mancini, M., Curi, N., Rafael, R.B.A., Cardelli, V., Cocco, S., Corti, G., Chakraborty, S., Li, B., Weindorf, D.C., 2021. PXRF in Tropical Soils: Methodology, Applications Achievements and Challenges. Adv. Agron. 167, 1–62. https://doi.org/10.1016/bs.agron.2020.12.001.

Soil Science Society of America, 2008. Glossary of Soil Science Terms 2008. Am. Soc. of Agronomy and Soil Sci. Soc. of Am.

Soil Survey Staff, 2014. Keys to soil taxonomy, 12th ed. United States Department of Agriculture Natural Resources Conservation Service.

Stevanato, M., Parolin, M., Camargo Filho, M., Parolin, E.S.P., 2021. Brazilian Paleosols: state of the art. Revista da ANPEGE. 17, 128–145. https://doi.org/10.5418/ra2021. v17i33.11897.

Stockmann, U., Cattle, S.R., Minasny, B., McBratney, A.B., 2016. Utilizing portable X-ray fluorescence spectrometry for in-field investigation of pedogenesis. Catena 139, 220–231. https://doi.org/10.1016/j.catena.2016.01.007.

Stradioto, M.R., Chang, H.K., 2020. Diagênese de Arenitos do Grupo Bauru no Estado de São Paulo. Cienc. e Nat. 42, e88.

Sun, F., Bakr, N., Dang, T., Pham, V., Weindorf, D.C., Jiang, Z., Li, H., Wang, Q., 2020. Enhanced soil profile visualization using portable X-ray fluorescence (PXRF) spectrometry. Geoderma 358, 1–11. https://doi.org/10.1016/j. geoderma.2019.113997.

Teixeira, A.F.S., Weindorf, D.C., Silva, S.H.G., Guilherme, L.R.G., Curi, N., 2018. Portable X-ray fluorescence (pXRF) spectrometry applied to the prediction of chemical attributes in Inceptisols under different land use. Cienc. e Agrotecnologia. 42, 501–512. https://doi.org/10.1590/1413-70542018425017518.

Weindorf, D.C., Chakraborty, S., 2016. Portable X-ray Fluorescence Spectrometry Analysis of Soils. Methods of Soil Anal. 84, 1384–1392. https://doi.org/10.1002/saj2.20151.

Wright, V.P., 1992. Paleosol Recognition: a guide to early diagenesis in terrestrial settings. In: Wolf, K.H., Chilingarian, G.V. Diagenesis, III: Developments in Sedimentology. 12, 591-619. https://doi.org/10.1016/S0070-4571(08)70574-0.

Zhang, Y., Hartemink, A.E., 2017. Sampling designs for soil organic carbon stock assessment of soil profiles. Geoderma 307, 220–230. https://doi.org/10.1016/j. geoderma.2017.08.013.